Annexing magic and tune-out wavelengths to the clock transitions of the alkaline-earth-metal ions

Jasmeet Kaur,* Sukhjit Singh, and Bindiya Arora†
Department of Physics, Guru Nanak Dev University, Amritsar, Punjab 143005, India

B. K. Sahoo‡
Atomic, Molecular, and Optical Physics Division, Physical Research Laboratory, Navrangpura, Ahmedabad 380009, India

(Received 13 September 2016; published 6 April 2017)

We present additional magic wavelengths (λ_{magic}) for the clock transitions in the alkaline-earth-metal ions, considering circular polarized light, aside from our previously reported values [Kaur *et al.*, Phys. Rev. A **92**, 031402(R) (2015)] for linearly polarized light. Contributions from the vector component to the dynamic dipole polarizabilities [$\alpha_d(\omega)$] of the atomic states associated with the clock transitions play major roles in the evaluation of these λ_{magic}, hence facilitating choosing circular polarization of lasers in the experiments. Moreover, the actual clock transitions in these ions are carried out among the hyperfine levels. The λ_{magic} values in these hyperfine transitions are estimated and found to be different from λ_{magic} for the atomic transitions due to different contributions coming from the vector and tensor parts of $\alpha_d(\omega)$. Importantly, we also present λ_{magic} values that depend only on the scalar component of $\alpha_d(\omega)$ for their uses in a specially designed trap geometry for these ions so that they can be used unambiguously among any hyperfine levels of the atomic states of the clock transitions. We also present $\alpha_d(\omega)$ values explicitly at 1064 nm for the atomic states associated with the clock transitions, which may be useful for creating high-field-seeking traps for the above ions using the Nd:YAG laser. The tune-out wavelengths at which the states would be free from the Stark shifts are also presented. Accurate values of the electric dipole matrix elements required for these studies are given and trends of electron correlation effects in determining them are also highlighted.

DOI: 10.1103/PhysRevA.95.042501

I. INTRODUCTION

Atomic clocks based on optical lattices are capable of proffering outstanding stable and accurate time-keeping devices. A fundamental feature of an optical lattice clock is that it interrogates an optical transition with controlled atomic motion [1]. At present, the most stable clock is based on the optical lattices of ^{87}Sr atoms with accuracy below 10^{-18} [2]. The unique feature of this clock is that the atoms are trapped at the wavelengths of an external electric field at which the differential light shift of an atomic transition nullifies. These wavelengths are commonly known as the magic wavelengths (λ_{magic}) [3]. However, ions provide more accurate atomic clocks since various systematics in the ions can be controlled better [4,5]. As a result, a number of ions, such as $^{27}Al^+$, $^{199}Hg^+$, $^{171}Yb^+$, $^{115}In^+$, $^{88}Sr^+$, $^{40}Ca^+$, $^{113}Cd^+$, etc., are under consideration for building accurate clocks. Among the various ions proposed for frequency standards [4,6–9], the alkaline-earth-metal ions possess an advantage that transitions required for cooling and repumping of ions and clock frequency measurement can be easily accessed using nonbulky solid-state or diode lasers [4]. Moreover, the presence of metastable D states in these ions, whose lifetimes range from milliseconds to several seconds, assist in carrying out measurements meticulously.

The recent development on measurement of λ_{magic} in a singly charged $^{40}Ca^+$ ion has now opened up a platform for the possibility of building up pure optical trapped ion clocks [10]. Optical lattices blended with unique features of optical transitions in an ionic system can revolutionize the secondary as well as primary frequency standards. However, the potential of the optical dipole trap perturbs the energy levels of the ion unevenly and the consistency of an ion optical clock depreciates. Therefore, knowledge of λ_{magic} values in these ions would be instrumental for constructing all-optical trapped ion clocks. These wavelengths can be found using accurate values of the dynamic dipole polarizabilities $\alpha_d(\omega)$ of the states associated with the clock transitions. Also, information on the dynamic [$\alpha_d(\omega)$] values, especially at which the ions are being trapped, will be of great significance. Improved atomic clocks will obviously benefit widely used technologies, including precise determination of fundamental constants [11], accurate control of quantum states [12], and advancement in communication, global positioning systems [13], etc.

Following the measurement of λ_{magic} in the $4S_{1/2}$-$3D_{5/2}$ transition of $^{43}Ca^+$, we had investigated these values in the $nS_{1/2}$–$(n-1)D_{3/2}$ and nS–$(n-1)D_{5/2}$ transitions of the alkaline-earth-metal ions [14] for the ground-state principal quantum number n. However, those studies were focused mainly on the linearly polarized light, limiting the choice for experimental measurements. Application of circular polarized light to atomic systems introduce contributions from the vector polarizabilities in the Stark shifts of the energy levels, which are linearly proportional to the angular frequency of the applied field. This can help in manipulating the Stark shifts in the energy levels and can lend to more degrees of freedom to attain further λ_{magic} values as per the experimental stipulation. Moreover, it is advantageous to consider hyperfine transitions in certain isotopes of the singly charged alkaline-earth-metal ions, giving rise to zero hyperfine angular momentum, to get rid off the systematics due to electric quadrupole shifts [15–17]. Since α_d values of atomic and hyperfine states in an atomic

*jasmeetphy.rsh@gndu.ac.in
†bindiya.phy@gndu.ac.in
‡bijaya@prl.res.in

system are different when vector and tensor components of α_d contribute, the $\lambda_{\rm magic}$ values also differ between the atomic and hyperfine transitions. Thus, it would be pertinent to investigate $\lambda_{\rm magic}$ both in the atomic and hyperfine transitions before the experimental consideration of the proposed ions. In fact, it could be more convenient to have $\lambda_{\rm magic}$ that are independent of choice of both magnetic and hyperfine sublevels in a given clock transition.

In fact, the Nd:YAG lasers at 1064 nm are often used for trapping atoms and ions because of their relatively high power and low intensity noise [18]. Traps built with long-wavelength lasers are generally high field seeking, where the atoms are attracted to the intensity maxima. Dynamic polarizabilities for the considered ions at 1064 nm will be of immense interest to the experimentalists since these polarizabilities will be immediately useful for operating optical traps at 1064-nm light fields.

In the present work, we aim to search for the $\lambda_{\rm magic}$ for the $nS_{1/2}$–$(n-1)D_{3/2,5/2}$ optical clock transitions, both in the atomic and hyperfine levels, in $^{43}Ca^+$ (with nuclear spin $I=7/2$), $^{87}Sr^+$ ($I=9/2$), and $^{137}Ba^+$ ($I=3/2$) ions using circularly polarized light. These values can be compared with the values for the linearly polarized light reported in Ref. [14] for the experimental consideration to trap the above ions. Also, we had demonstrated in a recent work how a trap geometry can be chosen in such a way that Stark shifts observed by the energy levels can be free from the contributions from the vector and tensor components of the α_d of the atomic states [19]. Assuming such trapping geometries for the considered alkaline-earth-metal ions, we also give $\lambda_{\rm magic}$ values using only the scalar polarizability contributions. Moreover, we identify the tune-out wavelengths ($\lambda_{\rm T}$) of the respective states for which the dynamic dipole polarizability of these ions vanishes. Comprehension of these $\lambda_{\rm T}$ values are needed for the sympathetic cooling of other possible singly and multiply charged ions in two-species mixtures with the considered alkaline-earth-metal ions [5,8,20]. We also present dynamic polarizability of these states at the 1064-nm wavelength of the applied external electric field. Contributions from various electric dipole ($E1$) matrix elements in determining the α_d values and the role of the electron correlation effects for the evaluation of accurate values of the $E1$ matrix elements are also discussed. Unless stated otherwise, all the results are given in atomic unit (a.u.) throughout this paper.

II. THEORY

The Stark shift in the energy of Kth level of an atom placed in an electric field is given by [21,22]

$$\Delta E^K = -\tfrac{1}{4}\alpha_d^K(\omega)\mathcal{E}^2, \tag{1}$$

where $\mathcal{E}$ is the amplitude of the external electric field due to the applied laser in an atomic system and $\alpha_d^K(\omega)$ is the dynamic dipole polarizability for the state K with its magnetic projection M. In tensor decomposition, α_d^K can be expressed as

$$\alpha_d^K(\omega) = \alpha_{d,0}^K(\omega) + \beta(\epsilon)\frac{M}{2K}\alpha_{d,1}^K(\omega) + \gamma(\epsilon)\frac{3M^2 - K(K+1)}{K(2K-1)}\alpha_{d,2}^K(\omega), \tag{2}$$

where $\alpha_{d,i}^K(\omega)$ with $i=0,1,2$ are the scalar, vector, and tensor components of $\alpha_d^K(\omega)$ respectively. In the specific cases, K can be either the atomic angular momentum J or hyperfine angular momentum F. The terms $\beta(\epsilon)$ and $\gamma(\epsilon)$ are defined as [23]

$$\beta(\epsilon) = \iota(\hat{\epsilon}\times\hat{\epsilon}^*)\cdot\hat{e}_B \tag{3}$$

and

$$\gamma(\epsilon) = \tfrac{1}{2}[3(\hat{\epsilon}^*\cdot\hat{e}_B)(\hat{\epsilon}\cdot\hat{e}_B) - 1], \tag{4}$$

with the quantization axis unit vector $\hat{e}_B$ and polarization unit vector $\hat{\epsilon}$. The differential Stark shift of a transition between states K to K' can be formulated as

$$\delta E_{KK'} = \Delta E_K - \Delta E_{K'} = -\frac{1}{2}\Bigg[\left\{\alpha_{d,0}^K(\omega) - \alpha_{d,0}^{K'}(\omega)\right\} + \beta(\epsilon)\left\{\frac{M_K}{2K}\alpha_{d,1}^K(\omega) - \frac{M_{K'}}{2K'}\alpha_{d,1}^{K'}(\omega)\right\} + \gamma(\epsilon)\left\{\frac{3M_K^2 - K(K+1)}{K(2K-1)}\alpha_{d,2}^K(\omega) - \frac{3M_{K'}^2 - K'(K'+1)}{K'(2K'-1)}\alpha_{d,2}^{K'}(\omega)\right\}\Bigg]\mathcal{E}^2. \tag{5}$$

To obtain null differential Stark shift, it is obvious from Eq. (5) that either the independent components of the polarizabilities cancel out each other or the net resultant nullifies, which depends upon the choice of $\beta(\epsilon)$, $\gamma(\epsilon)$, M_K, and $M'_{K'}$ magnetic sublevels. Moreover, as we have demonstrated recently, the differential Stark shift can be independent of the vector and tensor components of the states involved in a transition for a certain trap geometry [19]. Such trapping scheme is useful for M_J, F, and M_F insensitive trapping and can be suitably applied for considered clock transitions in alkaline-earth-metal ions.

Conveniently, the expressions for polarizabilities of the hyperfine and atomic levels can be expressed as [19]

$$\alpha_d^F(\omega) = \alpha_{d,0}^F(\omega) + \alpha_{d,1}^F(\omega)\frac{A\cos\theta_k M_F}{2F} + \alpha_{d,2}^F(\omega) \times\left(\frac{3\cos^2\theta_p - 1}{2}\right)\left[\frac{3M_F^2 - F(F+1)}{F(2F-1)}\right], \tag{6}$$

and

$$\alpha_d^J(\omega) = \alpha_{d,0}^J(\omega) + \alpha_{d,1}^J(\omega)\frac{A\cos\theta_k M_J}{2J} + \alpha_{d,2}^J(\omega) \times\left(\frac{3\cos^2\theta_p - 1}{2}\right)\left[\frac{3M_J^2 - J(J+1)}{J(2J-1)}\right], \tag{7}$$

where $\alpha_{d,i}^{K=J,F}(\omega)$ with $i=0,1,2$ are the scalar, vector, and tensor components of the respective polarizabilities, A represents degree of polarization, θ_k is the angle between the quantization axis and wave vector, and θ_p is the angle between the quantization axis and direction of polarization of the field. In the presence of a magnetic field, $\cos\theta_k$ and $\cos^2\theta_p$ can have any values depending on the direction of the applied magnetic field. In the absence of a magnetic field, $\cos\theta_k = 0$ and $\cos^2\theta_p = 1$ for the linearly polarized light, where polarization vector is assumed to be along the quantization axis. However, it yields $\cos\theta_k = 1$ and $\cos^2\theta_p = 0$ for the circularly polarized

light, where the wave vector is assumed to be along the quantization axis. Polarizabilities of the hyperfine states can be evaluated from the atomic state results using the relations [23,24]

$$\alpha^F_{d,0}(\omega) = \alpha^J_{d,0}(\omega), \tag{8}$$

$$\alpha^F_{d,1}(\omega) = (-1)^{J+F+I+1}\begin{Bmatrix} F & J & I \\ J & F & 1 \end{Bmatrix} \times\sqrt{\frac{F(2F+1)(2J+1)(J+1)}{J(F+1)}}\alpha^J_{d,1}(\omega), \tag{9}$$

and

$$\alpha^F_{d,2}(\omega) = (-1)^{J+F+I}\begin{Bmatrix} F & J & I \\ J & F & 2 \end{Bmatrix} \times\sqrt{\frac{F(2F-1)(2F+1)}{(2F+3)(F+1)}} \times\sqrt{\frac{(2J+3)(2J+1)(J+1)}{J(2J-1)}}\alpha^J_{d,2}(\omega). \tag{10}$$

Further, we can evaluate the atomic dipole polarizabilities using the expressions

$$\alpha^J_{d,0}(\omega) = \frac{2}{3(2J+1)}\sum_{J'}\frac{(E-E')|\langle J||\mathbf{D}||J'\rangle|^2}{\omega^2-(E-E')^2}, \tag{11}$$

$$\alpha^J_{d,1}(\omega) = \sqrt{\frac{24J}{(J+1)(2J+1)}}\sum_{J'}(-1)^{J+J'} \times\begin{Bmatrix} J & 1 & J \\ 1 & J' & 1 \end{Bmatrix}\frac{\omega|\langle J||\mathbf{D}||J'\rangle|^2}{\omega^2-(E-E')^2}, \tag{12}$$

and

$$\alpha^J_{d,2}(\omega) = \sqrt{\frac{40J(2J-1)}{3(J+1)(2J+3)(2J+1)}}\sum_{J'}(-1)^{J+J'} \times\begin{Bmatrix} J & 2 & J \\ 1 & J' & 1 \end{Bmatrix}\frac{(E-E')|\langle J||\mathbf{D}||J'\rangle|^2}{\omega^2-(E-E')^2}, \tag{13}$$

where J's are the angular momentum of the intermediate states, E and E' are energies of the corresponding states, and $\langle J||\mathbf{D}||J'\rangle$ are the reduced $E1$ matrix elements.

We define the tune-out wavelength λ_T as the wavelength where the dynamic polarizability of the state is zero. We have determined the tune-out wavelengths for the ground, $(n-1)D_{3/2}$ and $(n-1)D_{5/2}$ states of $^{43}Ca^+$, $^{87}Sr^+$, and $^{137}Ba^+$ ions. The detailed description about these calculations have been given in the Refs. [25,26].

III. METHOD OF EVALUATION

As discussed in our earlier works [14,27,28], each component of $\alpha^J_d(\omega)$ can be conveniently evaluated in the considered alkaline-earth-metal ions, in which many of the low-lying states have electronic configurations as a common closed core of inert gas atoms and a well-defined valence orbital, by classification into three different contributions, such as

$$\alpha^J_{d,i}(\omega) = \alpha^{J,c}_{d,i}(\omega) + \alpha^{J,cv}_{d,i}(\omega) + \alpha^{J,v}_{d,i}(\omega), \tag{14}$$

where $\alpha^{J,c}_{d,i}$, $\alpha^{J,cv}_{d,i}$, and $\alpha^{J,v}_{d,i}$ are referred to as the core, core-valence, and valence electron correlation contributions, respectively. Since the valence electron correlation effects are mainly estimated by $\alpha^{J,v}_{d,i}$, this gives a majority contribution followed by $\alpha^{J,c}_{d,i}$. Again, accuracies in the *ab initio* results of these quantities mainly suffer due to the uncertainties associated with the calculated energies of the atomic states. Therefore, we calculate only the $E1$ matrix elements of low-lying states of the considered ions employing a relativistic coupled-cluster (RCC) method, which is an all-order perturbative method, and combine them with the experimental energy values from the National Institute of Science and Technology (NIST) database [29] to determine the dominant contributions to $\alpha^{J,v}_{d,i}$. We refer this as the "main" contribution to $\alpha^{J,v}_{d,i}$, while the smaller contributions coming from the high-lying excited states are estimated in the *ab initio* formalism using the Dirac-Hartree-Fock (DHF) method and are mentioned as the "tail" contribution to $\alpha^{J,v}_{d,i}$. To estimate the other two contributions, it is not possible to use the sum-over-states approach, so we determine $\alpha^{J,c}_{d,i}$ in the random-phase approximation (RPA). This included core-polarization effects to all orders. It has been found that RPA can give these values reliably for the inert-gas-configured atomic systems [30]. Again, as demonstrated later, the $\alpha^{J,cv}_{d,i}$ contributions are very small in these ions. Thus, we evaluate them using the DHF method.

A small number of $E1$ matrix elements of the nD-nF transitions of $^{137}Ba^+$ are borrowed from the work of Sahoo *et al.* [31], while the rest of the $E1$ matrix elements for the evaluation of the "main" contribution to $\alpha^{J,v}_d$ are obtained considering the singles and doubles excitation approximation in the RCC (SD) method as described in Refs. [32,33]. In the SD method, the wave function of the state with the closed core with a valence electron v is represented as an expansion

$$|\Psi_v\rangle_{SD} = \left[1 + \sum_{ma}\rho_{ma}a^\dagger_m a_a + \frac{1}{2}\sum_{mnab}\rho_{mnab}a^\dagger_m a^\dagger_n a_b a_a + \sum_{m\neq v}\rho_{mv}a^\dagger_m a_v + \sum_{mna}\rho_{mnva}a^\dagger_m a^\dagger_n a_a a_v\right]|\Phi_v\rangle, \tag{15}$$

where $|\Phi_v\rangle$ is the DHF wave function of the state. In the above expression, $a^\dagger_i$ and a_i are the creation and annihilation operators with the indices $\{m,n\}$ and $\{a,b\}$ designating the virtual and core orbitals of $|\Phi_v\rangle$, ρ_{ma} and ρ_{mv} are the corresponding single-core and valence excitation coefficients, and ρ_{mnab} and ρ_{mnva} are the double-core and valence excitation coefficients. To obtain the DHF wave function, we use a finite-size basis set consisting of 70 B-splines constrained to a large cavity of radius $R = 220$ a.u. and solved self-consistently using the Roothan equation on a nonlinear grid.

In order to verify contributions from the higher level excitations, we also estimate leading-order contributions from the triple excitations perturbatively in the SD method framework (SDpT method) by expressing the atomic wave functions as

TABLE I. Calculated values of the static dipole polarizabilities $\alpha^J_{d,i}(0)$ for $nS_{1/2}$ and $(n-1)D_{3/2,5/2}$ states of $^{43}Ca^+$, $^{87}Sr^+$, and $^{137}Ba^+$ alkaline-earth-metal ions. Polarizability values are compared with the other available theoretical and experimental results. References are given in square brackets. Uncertainties in the results are given in parentheses.

	Ca^+				
$4S_{1/2}$ state		$3D_{3/2}$ state		$3D_{5/2}$ state	
	$\alpha^J_{d,0}$		$\alpha^J_{d,0}$	$\alpha^J_{d,2}$		$\alpha^J_{d,0}$	$\alpha^J_{d,2}$
$4P_{1/2}$	24.38(6)	$4P_{1/2}$	19.24(5)	−19.24(5)	$4P_{3/2}$	22.77(8)	−22.77(8)
$5P_{1/2}$	0.07	(5–7)$P_{1/2}$	0.011	−0.011	(5–7)$P_{3/2}$	0.016	−0.016
(6–7)$P_{1/2}$	0.01	$4P_{3/2}$	3.76	3.009	$4F_{5/2}$	0.12	0.14
$4P_{3/2}$	48.4(17)	(5–7)$P_{3/2}$	0.0027	0.002	$6F_{5/2}$	0.056	0.06
$5P_{3/2}$	0.01	$4F_{5/2}$	2.49(1)	−0.49	$4F_{5/2}$	2.39(14)	−0.85
(6–7)$P_{3/2}$	0.019	$5F_{5/2}$	0.81	−0.16	$5F_{7/2}$	0.76	−0.27
		$6F_{5/2}$	0.36	−0.07	$6F_{7/2}$	0.001	−0.0005
"Main" $\alpha^{J,v}_{d,i}$	72.88		26.67	−16.96		26.12	−23.71
$\alpha^{J,c}_{d,i}$	3.25		3.25			3.25	
"Tail" $\alpha^{J,v}_{d,i}$	5.86×10^{-2}		3.75	−0.75		3.75	−1.08
$\alpha^{J,cv}_{d,i}$	-8.85×10^{-2}		-7.94×10^{-3}			-1.02×10^{-2}	
$\alpha^J_{d,i}(0)$ (present)	76.1(2)		33.67(1.8)	−17.71		33.11(1.8)	−24.78(4)
$\alpha^J_{d,i}(0)$ (other) [37]	75.28		32.99	−17.88		32.81	−25.16
$\alpha^J_{d,i}(0)$ (other) [38]	73.0(1.5)		28.5(1.0)	−15.8(7)		29.5(1.0)	−22.45(5)
$\alpha^J_{d,i}(0)$ (other) [39]	75.49		32.73	−17.64		32.73	−25.20
$\alpha^J_{d,i}(0)$ (expt.) [40]	75.3(4)						
	Sr^+				
$5S_{1/2}$ state		$4D_{3/2}$ state		$4D_{5/2}$ state	
	$\alpha^J_{d,0}$		$\alpha^J_{d,0}$	$\alpha^J_{d,2}$		$\alpha^J_{d,0}$	$\alpha^J_{d,2}$
$5P_{1/2}$	29.47(10)	$5P_{1/2}$	38.67(2)	−38.67(2)	$5P_{3/2}$	44.16(3)	−44.16(3)
$6P_{1/2}$	0.0008	(6–8)$P_{1/2}$	0.0063	−0.0063	(6–8)$P_{3/2}$	0.015	−0.015
(7–8)$P_{1/2}$	0.071	$5P_{3/2}$	7.024(2)	5.62(2)	$4F_{5/2}$	0.33	0.37
$5P_{3/2}$	56.93(27)	(6–8)$P_{3/2}$	0.003	0.002	$6F_{5/2}$	0.12	0.13
$6P_{3/2}$	0.0015	$4F_{5/2}$	6.63(7)	−1.33	$4F_{5/2}$	6.51(5)	−2.32(2)
(7–8)$P_{3/2}$	0.0058	$5F_{5/2}$	1.76	−0.35	$5F_{7/2}$	1.72	−0.61
		$6F_{5/2}$	0.72	−0.14	$6F_{7/2}$	0.69	−0.25
"Main" $\alpha^{J,v}_{d,i}$	86.47		54.81	−34.88		53.55	−46.85
$\alpha^{J,c}_{d,i}$	4.98		4.98			4.98	
"Tail" $\alpha^{J,v}_{d,i}$	1.96×10^{-2}		4.94	−1.0		4.96	−1.44
$\alpha^{J,cv}_{d,i}$	−0.19		-1.77×10^{-3}			-2.78×10^{-2}	
$\alpha^J_{d,i}(0)$ (present)	91.23(0.3)		64.7(2.5)	−35.88(5)		63.5(2.5)	−48.29(7)
$\alpha^J_{d,i}(0)$ (other) [41]	89.99		61.77			61.77	
$\alpha^J_{d,i}(0)$ (other) [15]	88.29(1.0)		61.43(52)	35.42		62.87(75)	−48.83(30)
$\alpha^J_{d,i}(0)$ (expt.) [42]	93.3(9)		57.0			57.0	
	Ba^+				
$6S_{1/2}$ state		$5D_{3/2}$ state		$5D_{5/2}$ state	
	$\alpha^J_{d,0}$		$\alpha^J_{d,0}$	$\alpha^J_{d,2}$		$\alpha^J_{d,0}$	$\alpha^J_{d,2}$
$6P_{1/2}$	40.23(14)	$6P_{1/2}$	22.51(13)	−22.51(13)	$6P_{3/2}$	25.66(1)	−25.66(1)
$7P_{1/2}$	0.005	(7–8)$P_{1/2}$	0.075	−0.074	(7–8)$P_{3/2}$	0.13	−0.13
$8P_{1/2}$	0.009	$6P_{3/2}$	3.86	3.095	$4F_{5/2}$	0.668(5)	0.763(2)
$6P_{3/2}$	73.93(4)	(7–8)$P_{3/2}$	0.023	0.018	(5–6)$F_{5/2}$	0.0955(1)	0.109(2)
$7P_{3/2}$	0.011	$4F_{5/2}$	11.85(3)	−2.37	$4F_{7/2}$	13.34(13)	−4.76(5)
$8P_{3/2}$	0.013	(5–6)$F_{5/2}$	1.76	−0.35	$5F_{7/2}$	2.863(34)	−1.022(17)
"Main" $\alpha^{J,v}_{d,i}$	114.19		40.07	−22.19		42.76	−30.71
$\alpha^{J,c}_{d,i}$	9.35		9.35			9.35	
"Tail" $\alpha^{J,v}_{d,i}$	1.66×10^{-2}		4.75	−1.0		4.79	−1.46
$\alpha^{J,cv}_{d,i}$	−0.37		-2.34×10^{-2}			-3.87×10^{-2}	
$\alpha^J_{d,i}(0)$ (present)	123.7(5)		54.17(2.5)	−22.19(4)		56.87(2.4)	−32.17(3)
$\alpha^J_{d,i}(0)$ (other) [15]	124.26(1.0)		48.81(46)	−24.62(28)		50.67(58)	−30.85(31)
$\alpha^J_{d,i}(0)$ (other) [43]	123.88(5)						

[32,34]

$$|\Psi_v\rangle_{\rm SDpT} = |\Psi_v\rangle_{\rm SD} + \frac{1}{6}\sum_{mnrab}\rho^{pert}_{mnrvab}a^\dagger_m a^\dagger_n a^\dagger_r a_b a_a a_v|\Phi_v\rangle, \tag{16}$$

where ρ^{pert}_{mnrvab} is the perturbed triple valence excitation amplitudes.

After obtaining wave functions employing the SD and SDpT methods, we determine the $E1$ matrix element for a given transition between the states $|\Psi_v\rangle$ and $|\Psi_w\rangle$ by evaluating the expression

$$Z_{vw} = \frac{\langle\Psi_v|Z|\Psi_w\rangle}{\sqrt{\langle\Psi_v|\Psi_v\rangle\langle\Psi_w|\Psi_w\rangle}}. \tag{17}$$

To find out the uncertainties with the calculated $E1$ matrix elements, we have carried out semiempirical scaling of the wave functions that accounts for evaluation of missing correlations contributions to the wave functions from the approximated SD and SDpT methods. This procedure involves

TABLE II. Calculated values of the dynamic dipole polarizabilities $\alpha^J_{d,i}(\omega)$ for the $nS_{1/2}$ and $(n-1)D_{3/2,5/2}$ states of $^{43}Ca^+$, $^{87}Sr^+$, and $^{137}Ba^+$ ions at $\lambda = 1064$ nm (equivalent to $\omega \simeq 0.035$ a.u.). Uncertainties in the results are given in parentheses.

				Ca^+					
	$4S$ state			$3D_{3/2}$ state				$3D_{5/2}$ state	
	$\alpha^J_{d,0}$	$\alpha^J_{d,1}$		$\alpha^J_{d,0}$	$\alpha^J_{d,1}$	$\alpha^J_{d,2}$		$\alpha^J_{d,0}$	$\alpha^J_{d,1}$	$\alpha^J_{d,2}$
$4P_{1/2}$	28.33(7)	−21.141(5)	$4P_{1/2}$	57.12(2)	−139.55(3)	−57.12(2)	$4P_{3/2}$	64.13(2)	−154.55(5)	−64.13(2)
$5P_{1/2}$	0.0072	−0.002	$(5–7)P_{1/2}$	0.011	−0.007	−0.011	$(5–7)P_{3/2}$	0.016	−0.009	−0.016
$(6–7)P_{1/2}$	0.011	−0.0027	$4P_{3/2}$	8.59(1)	−8.24	6.87	$4F_{5/2}$	0.12	−0.018	0.14
$4P_{3/2}$	56.03(20)	20.719	$(5–7)P_{3/2}$	0.0028	−0.0006	0.0020	$(5–6)F_{5/2}$	0.056	−0.006	0.06
$5P_{3/2}$	0.01	0.002	$4F_{5/2}$	2.57(1)	0.79	−0.51	$4F_{5/2}$	2.46(12)	0.91	−0.88
$(6–7)P_{3/2}$	0.019	0.003	$5F_{5/2}$	0.82	0.22	−0.16	$5F_{7/2}$	0.78	0.24	−0.27
			$6F_{5/2}$	0.37	0.09	−0.07	$6F_{7/2}$	0.001	0.0004	−0.0005
"Main" $\alpha^{J,v}_{d,i}$	84.4	−0.423		69.5	−146.69	−50.9		67.5	−153.37	−65.1
$\alpha^{J,c}_{d,i}$	3.25			3.25				3.25		
"Tail" $\alpha^{J,v}_{d,i}$	5.90×10^{-2}	-3.49×10^{-4}		3.79	0.73	−0.76		3.80	0.81	−1.09
$\alpha^{J,cv}_{d,i}$	-8.85×10^{-2}			-7.94×10^{-3}				-1.02×10^{-2}		
$\alpha^J_{d,i}(\omega)$	87.6(2)	−0.423		76.5(1.9)	−145.96(0.36)	−51.7(3)		74.6(1.9)	−152.56(0.41)	−66.0(5)
				Sr^+					
	$5S$ state			$4D_{3/2}$ state				$4D_{5/2}$ state	
	$\alpha^J_{d,0}$	$\alpha^J_{d,1}$		$\alpha^J_{d,0}$	$\alpha^J_{d,1}$	$\alpha^J_{d,2}$		$\alpha^J_{d,0}$	$\alpha^J_{d,1}$	$\alpha^J_{d,2}$
$5P_{1/2}$	34.96(12)	−27.714(9)	$5P_{1/2}$	−730.9(4)	2250.05(1.3)	730.9(4)	$5P_{3/2}$	769.4(5)	−2241.08(1.6)	−769.4(5)
$6P_{1/2}$	0.0008	−0.0003	$(6–8)P_{1/2}$	−0.007	−0.005	−0.007	$(6–8)P_{3/2}$	0.016	−0.01	−0.016
$(7–8)P_{1/2}$	0.007	−0.002	$5P_{3/2}$	64.03(2)	−72.49(2)	51.22(2)	$4F_{5/2}$	0.34	−0.059	0.38
$5P_{3/2}$	66.74(32)	25.58(1)	$(6–8)P_{3/2}$	0.003	−0.0008	0.002	$(5–6)F_{5/2}$	0.12	−0.02	0.5
$6P_{3/2}$	0.0046	0.0003	$4F_{5/2}$	6.91(7)	2.52	−1.38	$4F_{5/2}$	6.79(5)	2.96	−2.42(2)
$(7–8)P_{3/2}$	0.0029	0.0008	$5F_{5/2}$	1.81	0.54	−0.36	$5F_{7/2}$	1.76	0.63	−0.63
			$6F_{5/2}$	0.73	0.22	−0.15	$6F_{7/2}$	0.71	0.23	−0.25
"Main" $\alpha^{J,v}_{d,i}$	101.7	−2.13		−657.4	2180.82	780.2		779.1	−2237.34	−771.8
$\alpha^{J,c}_{d,i}$	4.98			4.98				4.98		
"Tail" $\alpha^{J,v}_{d,i}$	1.96×10^{-2}	-8.13×10^{-4}		5.05	1.11	−1.02		5.05	1.24	−1.46
$\alpha^{J,cv}_{d,i}$	−0.19			-1.77×10^{-3}				-2.79×10^{-2}		
$\alpha^J_{d,i}(\omega)$	106.52(3)	−2.14		−647.4(3)	2181.92(1.79)	779.2(6)		789.2(2.6)	−2236.10(2.82)	−773.(9)
				Ba^+					
	$6S$ state			$5D_{3/2}$ state				$5D_{5/2}$ state	
	$\alpha^J_{d,0}$	$\alpha^J_{d,1}$		$\alpha^J_{d,0}$	$\alpha^J_{d,1}$	$\alpha^J_{d,2}$		$\alpha^J_{d,0}$	$\alpha^J_{d,1}$	$\alpha^J_{d,2}$
$6P_{1/2}$	51.26(18)	−47.55(2)	$6P_{1/2}$	35.89(2)	−65.77(4)	−35.89(2)	$6P_{3/2}$	38.5(2)	−66.08(3)	−38.5(2)
$7P_{1/2}$	0.006	−0.002	$(7–8)P_{1/2}$	0.077	−0.05	−0.077	$(7–8)P_{3/2}$	0.13	−0.08	−0.13
$8P_{1/2}$	0.009	−0.003	$6P_{3/2}$	5.55	−3.66(2)	4.44	$4F_{5/2}$	0.70	−0.13	0.80
$6P_{3/2}$	90.52(4)	38.75(2)	$(7–8)P_{3/2}$	0.024	−0.005	0.019	$(5–6)F_{5/2}$	0.107(1)	−0.02	0.122(2)
$7P_{3/2}$	0.011	0.002	$4F_{5/2}$	12.44(3)	4.85	−2.48	$4F_{7/2}$	14.02(14)	6.59	−5.007(5)
$8P_{3/2}$	0.013	0.002	$(5–6)F_{5/2}$	1.83	0.5	−0.36	$5F_{7/2}$	3.41(2)	1.29	−1.22
"Main" $\alpha^{J,v}_{d,i}$	141.81	−8.80		55.8	−64.05	−34.35		56.86	−59.02	−43.9
$\alpha^{J,c}_{d,i}$	9.35			9.35				9.35		
"Tail" $\alpha^{J,v}_{d,i}$	1.67×10^{-2}	-1.24×10^{-4}		3.29	0.7	−0.71		3.31	0.77	−1.04
$\alpha^{J,cv}_{d,i}$	−0.37			-2.35×10^{-2}				-3.88×10^{-2}		
$\alpha^J_{d,i}(\omega)$	150.6(5)	−8.80		68.44(1.7)	−63.55(0.35)	−35.05(4)		69.52(1.7)	−58.25(0.38)	−44.97(5)

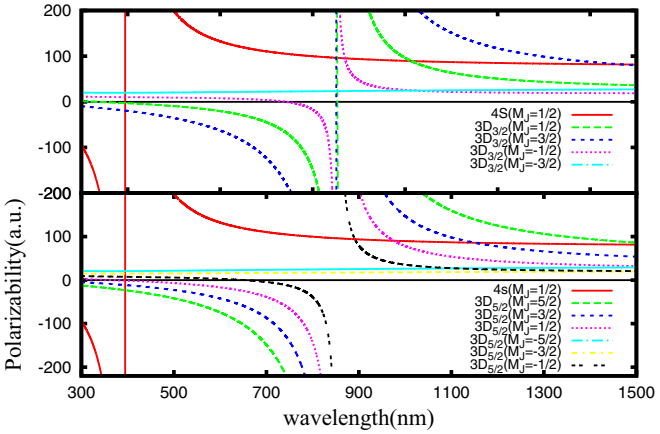

FIG. 1. Dynamic dipole polarizabilities (in a.u.) for the $4S_{1/2}$ and $3D_{3/2,5/2}$ states of $^{43}Ca^{+}$ with $A = -1$.

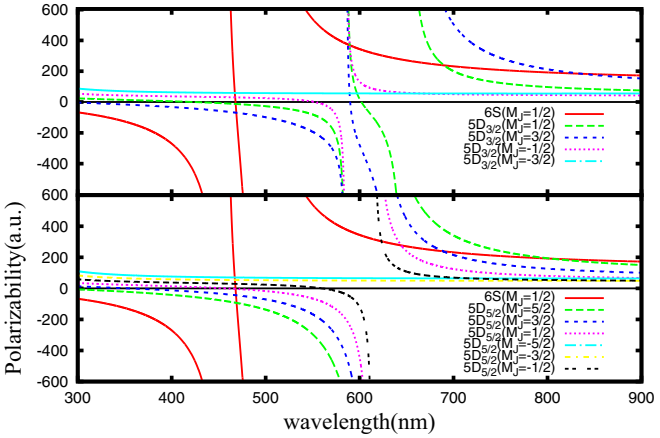

FIG. 3. Dynamic dipole polarizabilities (in a.u.) for the $6S_{1/2}$ and $5D_{3/2,5/2}$ states of $^{137}Ba^{+}$ with $A = -1$.

scaling of the excitation coefficients and reevaluation of the $E1$ matrix elements. The scaling factors are decided from the correlation energy trends in the SD and SDpT methods. Details regarding this scaling procedure are given in Ref. [35].

IV. RESULTS AND DISCUSSION

Since valence correlation contributions are vital for accurate estimate of polarizabilities, we include the $E1$ matrix elements among the low-lying states up to $4S$-$7P$, $3D$-$7P$, and $3D$-$6F$ transitions in $^{43}Ca^{+}$, $5S$-$8P$, $4D$-$8P$, and $4D$-$6F$ transitions in $^{87}Sr^{+}$ and $6S$-$8P$, $5D$-$8P$, and $5D$-$6F$ transitions in $^{137}Ba^{+}$ for the evaluation of the "main" contributions. All these matrix elements are calculated using the RCC method described in the previous section. A few $E1$ matrix elements of the nD-nF transitions of $^{137}Ba^{+}$ are used from Ref. [31]. We present these considered $E1$ matrix elements in the Supplemental Material [36] from different levels of approximation in the considered many-body methods. Scaled values to the SD and SDpT results, which mainly ameliorate the results by accounting for corrections beyond the Brueckner-orbital contributions [32], are also given in the tables of the Supplemental Material. We then give the "final" results considering the most reliable values along with their estimated uncertainties in parentheses in the last column of this table [44]. As can be seen from the Supplemental Material, the DHF method gives large $E1$ matrix element values while the SD method brings down the values while the SDpT method slightly increases the values from the SD values. The scaled values from both the SD and SDpT methods modify these values marginally. Thus, these values seem to be very reliable for determining the polarizabilities of the considered ions. For the final use, we recommend the SD method values and uncertainties to these values are estimated by taking the differences from the results obtained using the SDpT method. Below, we discuss polarizability results using these $E1$ matrix elements and magic wavelengths of the $S - D$ clock transitions of the above alkaline-earth-metal ions.

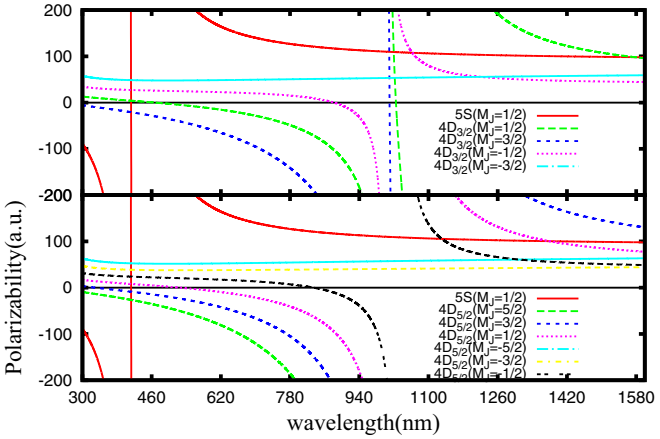

FIG. 2. Dynamic dipole polarizabilities (in a.u.) for the $5S_{1/2}$ and $4D_{3/2,5/2}$ states of $^{87}Sr^{+}$ with $A = -1$.

A. Static polarizability results

Using the $E1$ matrix elements given in Supplemental Material [36], we first evaluate the static polarizabilities of the ground and $(n-1)D_J$ states of the $^{43}Ca^{+}$, $^{87}Sr^{+}$, and $^{137}Ba^{+}$ ions and compare them with the previously available experimental and theoretical results in Table I. We give both the scalar and tensor polarizabilities of the considered ground and $(n-1)D_J$ states along with their contributions from "main" and "tail" to valence $\alpha^{J,v}_{d,i}$, core-valence $\alpha^{J,cv}_{d,i}$, and core $\alpha^{J,c}_{d,i}$ contributions to our calculations in this table. These results are discussed ion-wise below.

1. $^{43}Ca^{+}$

As can be seen from Table I, $\alpha^{J}_{d,i}(0)$ value of 76.1(2) a.u. for the ground-state polarizability obtained for $^{43}Ca^{+}$ ion is in close agreement with the other theoretical calculations, which are 75.28 and 75.49 a.u. by Tang *et al.* [37] and Mitroy *et al.* [39], respectively. Mitroy *et al.* have also given these values in the $3D_{3/2}$ and $3D_{5/2}$ states of Ca^{+}. They had evaluated these polarizabilities by diagonalizing a semiempirical Hamiltonian constructed in a large-dimension single-electron basis. Our estimated values agree quite well those values within the quoted error bars. In Ref. [38], *ab initio* calculations of these quantities are reported using a RCC method and our values are also compare reasonably well with them. The most stringent

experimental value for the $^{43}Ca^{+}$ ground-state polarizability was obtained by spectral analysis in Ref. [40]; our result is also in agreement with this value.

2. $^{87}Sr^{+}$

Next, we compare our polarizability results for the $^{87}Sr^{+}$ ion given in Table I. The RCC results of the S and D states reported by Sahoo *et al.* [15] are in agreement with our values. Mitroy *et al.* have also given these values by employing a nonrelativistic method in the sum-over-states approach [41]. It can be seen from Table I that our ground-state dipole polarizability is in very good agreement with their result. However, it seems inappropriate to compare their nonrelativistic values for the dipole polarizabilities of the $4D_J$ states with our relativistic calculations. The estimate for the ground-state static polarizability of $^{87}Sr^{+}$ by Barklem *et al.* [41] was derived by combining their theoretical calculations with the experimental data from Ref. [42]. There is a considerable discrepancy between their result and our present value. This is mainly because of omission of the core contribution which has been included by us using the RPA method. There are no direct experimental results available for the Sr^{+} ion dipole polarizabilities to make a comparative analysis with the theoretical values.

3. $^{137}Ba^{+}$

Our precise ground-state polarizability calculation gives a value of 123.2(5) a.u. for the $^{137}Ba^{+}$ ion, which is in good agreement with the high-precision measurement achieved by a technique based on the resonant excitation Stark ionization spectroscopy [43]. We also expect that results of the $5D_J$ states will also be of similar accuracies in this ion.

Having analyzed accuracies of the static polarizabilities satisfactorily, we now move on to present the dynamic polarizabilities in the above ions. We adopt the similar procedures for calculations of these quantities, thus anticipating similar accuracies in the dynamic polarizability values as their corresponding static values. This allows us to determine the $\lambda_{\rm magic}$ values of the nS–$(n-1)D_{3/2}$, nS–$(n-1)D_{5/2}$ transitions and the $\lambda_{\rm T}$ values of the associated states in the alkaline-earth-metal ions without much qualm using these dynamic polarizabilities.

B. Dynamic dipole polarizabilities at 1064 nm

We are discussing here the dynamic polarizabilities at 1064 nm that are very demanding for creating high-field-seeking traps of the considered ions (far-detuned traps), where the atoms are attracted to the intensity maxima. Recently Chen *et al.* [45] had carried out measurements of scalar and tensor contributions to the atomic polarizabilities in the Rb atom at this wavelength. In our calculation of dynamic polarizabilities in the considered $^{43}Ca^{+}$, $^{87}Sr^{+}$, and $^{137}Ba^{+}$ ions, we have used same $E1$ matrix elements to determine the "main" contributions and estimated other nondominant contributions in the similar procedure as was done for the evaluation of the

TABLE III. The $\lambda_{\rm magic}$ values (in nm) with their corresponding polarizabilities $\alpha_d^J(\lambda_{\rm magic})$ (in a.u.) for the $nS_{1/2}(M_J = 1/2) \rightarrow (n-1)D_{3/2}$ transitions using circularly polarized light in the $^{43}Ca^{+}$, $^{87}Sr^{+}$, and $^{137}Ba^{+}$ ions. The resonant wavelengths $\lambda_{\rm res}$ to indicate the placement of the $\lambda_{\rm magic}$ in between resonant transitions are also listed.

		$M_J = 3/2$		$M_J = 1/2$		$M_J = -1/2$		$M_J = -3/2$	
Resonances	$\lambda_{\rm res}$	$\lambda_{\rm magic}$	$\alpha_d^J(\lambda_{\rm magic})$	$\lambda_{\rm magic}$	$\alpha_d^J(\lambda_{\rm magic})$	$\lambda_{\rm magic}$	$\alpha_d^J(\lambda_{\rm magic})$	$\lambda_{\rm magic}$	$\alpha_d^J(\lambda_{\rm magic})$
$^{43}Ca^{+}$	$4S_{1/2}$-$3D_{3/2}$								
$4S_{1/2}$-$4P_{3/2}$	393.366								
		394.6(4)	−20.34	394.6(9)	−2.82	394.6(10)	11.68	394.6(10)	22.40
$4S_{1/2}$-$4P_{1/2}$	396.847								
$3D_{3/2}$-$4P_{3/2}$	849.802								
		850.9(2)	96.33	853.1(2)	96.20				
$3D_{3/2}$-$4P_{1/2}$	866.214								
		1467.8(4)	81.31	1013.4(5)	89.31	870.7(3)	95.15		
$^{87}Sr^{+}$	$5S_{1/2}$-$4D_{3/2}$								
$5S_{1/2}$-$5P_{3/2}$	407.7714								
		412.5(9)	−20.62	412.4(9)	3.99	412.4(9)	27.18	412.3(8)	48.55
$5S_{1/2}$-$5P_{1/2}$	421.5524								
$4D_{3/2}$-$5P_{3/2}$	1003.6654								
		1009.3(2)	109.74	1019.7(3)	109.29	1062.5(3)	107.65		
$4D_{3/2}$-$5P_{1/2}$	1091.4874								
				1577.2(3)	98.17				
$^{137}Ba^{+}$	$6S_{1/2}$-$5D_{3/2}$								
$6S_{1/2}$-$6P_{3/2}$	455.4033								
		468.8(4)	−70.91	468.1(4)	−13.13	467.6(5)	30.14	467.3(4)	59.27
$6S_{1/2}$-$6P_{1/2}$	493.4077								
$5D_{3/2}$-$6P_{3/2}$	585.3675								
		587.6(9)	373.89	589.5(3)	368.60	589.6(5)	368.35		
$5D_{3/2}$-$6P_{1/2}$	649.6898								
		841.7(5)	182.54	690.7(7)	237.64				

TABLE IV. The λ_{magic} values (in nm) with their corresponding polarizabilities $\alpha_d^J(\lambda_{magic})$ (in a.u.) for the $nS_{1/2}(M_J = -1/2) \rightarrow (n-1)D_{3/2}$ transitions using circularly polarized light in the $^{43}Ca^+$, $^{87}Sr^+$, and $^{137}Ba^+$ ions. The resonant wavelengths λ_{res} to indicate the placement of the λ_{magic} in between resonant transitions are also listed.

		$M_J = 3/2$		$M_J = 1/2$		$M_J = -1/2$		$M_J = -3/2$	
Resonances	λ_{res}	λ_{magic}	$\alpha_d^J(\lambda_{magic})$	λ_{magic}	$\alpha_d^J(\lambda_{magic})$	λ_{magic}	$\alpha_d^J(\lambda_{magic})$	λ_{magic}	$\alpha_d^J(\lambda_{magic})$
$^{43}Ca^+$	$4S_{1/2}$-$3D_{3/2}$								
$3D_{3/2}$-$4P_{3/2}$	849.802								
		851.2(3)	95.63	853.5(4)	95.49				
$3D_{3/2}$-$4P_{1/2}$	866.214								
		1549.9(5)	80.95	1031.4(4)	88.28	875.56(2)	94.27		
$^{87}Sr^+$	$5S_{1/2}$-$4D_{3/2}$								
$5S_{1/2}$-$5P_{3/2}$	407.7714								
		416.9(7)	−21.20	416.8(5)	3.93	416.8(8)	27.12	416.7(8)	48.44
$5S_{1/2}$-$5P_{1/2}$	421.5524								
		442.5(5)	−25.36	442.3(6)	1.94	442.1(2)	26.46	441.9(4)	48.03
		478.2(5)	−31.49	479.2(4)	−0.96	480.1(2)	25.56	481.1(1)	47.83
$4D_{3/2}$-$5P_{3/2}$	1003.6654								
		1009.2(1)	106.69	1019.8(6)	106.29	1064.8(5)	104.79		
$4D_{3/2}$-$5P_{1/2}$	1091.4874								
				1593.1(5)	96.54				
$^{137}Ba^+$	$6S_{1/2}$-$5D_{3/2}$								
$6S_{1/2}$-$6P_{3/2}$	455.4033								
		479.2(5)	−79.42	478.5(4)	−17.21	477.9(1)	28.76	477.5(2)	58.89
$6S_{1/2}$-$6P_{1/2}$	493.4077								
		505.4(1)	−106.86	505.1(4)	−30.87	504.8(2)	24.05	504.7(2)	57.93
		571.4(4)	−314.04	574.1(2)	−213.32	577.3(4)	−125.29		
$5D_{3/2}$-$6P_{3/2}$	585.3675								
		589.4(4)	47.82	595.5(2)	89.44	602.4(2)	120.417	590.5(2)	56.46
$5D_{3/2}$-$6P_{1/2}$	649.6898								
		899.9(5)	153.13	710.5(4)	176.48				

TABLE V. The λ_{magic} values (in nm) with their corresponding polarizabilities $\alpha_d^J(\lambda_{magic})$ (in a.u.) for the $nS_{1/2}(M_J = 1/2) \rightarrow (n-1)D_{5/2}$ transitions using circularly polarized light in the $^{43}Ca^+$, $^{87}Sr^+$, and $^{137}Ba^+$ ions. The resonant wavelengths λ_{res} to indicate the placement of the λ_{magic} in between resonant transitions are also listed.

		$M_J = 5/2$		$M_J = 3/2$		$M_J = 1/2$		$M_J = -1/2$		$M_J = -3/2$		$M_J = -5/2$	
Resonances	λ_{res}	λ_{magic}	$\alpha_d^J(\lambda_{magic})$	λ_{magic}	$\alpha_d^J(\lambda_{magic})$	λ_{magic}	$\alpha_d^J(\lambda_{magic})$	λ_{magic}	$\alpha_d^J(\lambda_{magic})$	λ_{magic}	$\alpha_d^J(\lambda_{magic})$	λ_{magic}	$\alpha_d^J(\lambda_{magic})$
$^{43}Ca^+$	$4S_{1/2}$-$3D_{5/2}$												
$4S_{1/2}$-$4P_{3/2}$	393.366												
		394.64(2)	−25.67	394.64(3)	−9.69	394.64(2)	1.0	394.63(4)	6.33	394.63(3)	17.0	394.63(3)	22.39
$4S_{1/2}$-$4P_{1/2}$	396.847												
$3D_{5/2}$-$4P_{3/2}$	854.209												
				1150.39(2)	85.95	975.6(4)	90.54	891.4(3)	94.09				
$^{87}Sr^+$	$5S_{1/2}$-$4D_{5/2}$												
$5S_{1/2}$-$5P_{3/2}$	407.7714												
		412.5(3)	−26.94	412.46(2)	−10.05	412.42(4)	6.98	412.38(4)	24.16	412.35(3)	37.15	412.31(3)	54.61
$5S_{1/2}$-$5P_{1/2}$	421.5524												
$4D_{5/2}$-$5P_{3/2}$	1032.7309												
						1379.4(3)	100.44	1130.8(4)	105.46				
$^{137}Ba^+$	$6S_{1/2}$-$5D_{5/2}$												
$6S_{1/2}$-$6P_{3/2}$	455.4033												
		469.1(5)	−95.43	468.5(1)	−45.31	467.9(4)	−3.93	467.6(4)	29.01	467.3(1)	53.75	467.1(1)	70.27
$6S_{1/2}$-$6P_{1/2}$	493.4077												
$5D_{5/2}$-$6P_{3/2}$	614.1713												
		810.1(8)	189.71	691(2)	237.75	644.7(5)	275.99	623.3(5)	302.79				

TABLE VI. The λ_{magic} values (in nm) with their corresponding polarizabilities $\alpha_d^J(\lambda_{magic})$ (in a.u.) for the $nS_{1/2}(M_J=-1/2)\rightarrow(n-1)D_{5/2}$ transitions using circularly polarized light in the $^{43}Ca^+$, $^{87}Sr^+$, and $^{137}Ba^+$ ions. The resonant wavelengths λ_{res} to indicate the placement of the λ_{magic} in between resonant transitions are also listed.

		$M_J=5/2$		$M_J=3/2$		$M_J=1/2$		$M_J=-1/2$		$M_J=-3/2$		$M_J=-5/2$	
Resonances	λ_{res}	λ_{magic}	$\alpha_d^J(\lambda_{magic})$	λ_{magic}	$\alpha_d^J(\lambda_{magic})$	λ_{magic}	$\alpha_d^J(\lambda_{magic})$	λ_{magic}	$\alpha_d^J(\lambda_{magic})$	λ_{magic}	$\alpha_d^J(\lambda_{magic})$	λ_{magic}	$\alpha_d^J(\lambda_{magic})$
$^{43}Ca^+$	$4S_{1/2}$-$3D_{5/2}$												
$4S_{1/2}$-$4P_{1/2}$	396.847												
$3D_{5/2}$-$4P_{3/2}$	854.209												
				1173.5(2)	85.12	982.7(2)	89.77	893.4(3)	93.37				
$^{87}Sr^+$	$5S_{1/2}$-$4D_{5/2}$												
$5S_{1/2}$-$5P_{3/2}$	407.7714												
		416.93(4)	−27.93	416.88(3)	−9.02	416.85(4)	7.66	416.81(4)	23.82	416.77(1)	38.63	416.74(3)	52.53
$5S_{1/2}$-$5P_{1/2}$	421.5524												
		442.49(4)	−31.93	442.36(3)	−12.11	442.25(3)	6.12	442.13(4)	22.84	442.03(8)	38.18	441.93(3)	52.07
		477.99(5)	39.14	478.85(1)	−16.77	479.32(7)	3.55	479.98(9)	21.77	480.65(1)	37.83	481.28(7)	51.73
$4D_{5/2}$-$5P_{3/2}$	1032.7309												
						1391.4(3)	98.46	1134.5(4)	102.92				
$^{137}Ba^+$	$6S_{1/2}$-$5D_{5/2}$												
$6S_{1/2}$-$6P_{3/2}$	455.4033												
		479.5(2)	−108.02	478.9(2)	−52.89	478.4(2)	−7.78	477.9(4)	27.52	477.6(4)	53.33	477.4(7)	69.73
$6S_{1/2}$-$6P_{1/2}$	493.4077												
		505.5(2)	−149.78	505.3(4)	−78.36	505.04(41)	−20.96	504.8(4)	25.56	504.76(4)	52.23	504.69(7)	68.53
		568.8(2)	−451.72	572.14(2)	−284.62	576.52(2)	−144.27	582.4(2)	−31.07	589.7(4)	50.45	591.7(2)	65.99
$5D_{5/2}$-$6P_{3/2}$	614.1713												
		894.3(8)	153.62	729.9(2)	173.67	665.9(3)	180.26	632.6(5)	171.84				

static polarizabilities. We list the contributions to the $nS_{1/2}$ and $(n-1)D_J$ dynamic polarizabilities at this wavelength of the above ions in Table II. The dominant contributions are listed explicitly. This table illustrates very fast convergence of the $nS_{1/2}$ state polarizabilities from which we find that the largest contributions are appearing from the nP excited states. We also notice that contributions from the $4D_{3/2}$-$5P_{1/2}$ transition to the $4D_J$ state polarizabilities in $^{87}Sr^+$ increase 20 times as compared to the contribution from this transition to the $4D_J$ state static polarizability. The reason for the overwhelming contribution from this particular transition is due to the proximity of the $4D_{3/2}$-$5P_{1/2}$ resonance that lies at 1091 nm to the laser wavelength of 1064 nm.

C. Magic and tune-out wavelengths for circularly polarized light

In order to find out λ_{magic} among the (J,M_J) levels of the $nS_{1/2}\rightarrow(n-1)D_{3/2}$ and $nS_{1/2}\rightarrow(n-1)D_{5/2}$ transitions, we plot total dynamic dipole polarizabilities for the $nS_{1/2}$ and $(n-1)D_{3/2,5/2}$ states in Figs. 1, 2, and 3 for the $^{43}Ca^+$, $^{87}Sr^+$, and $^{137}Ba^+$ ions respectively. The λ_{magic} for the clock

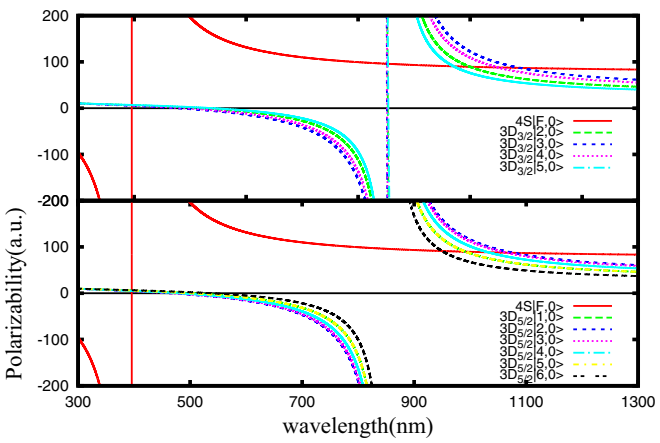

FIG. 4. F-dependent dynamic dipole polarizabilities (in a.u.) for the $|4S_{1/2}FM_F=0\rangle$ ($F=3$, 4) and $|3D_{3/2,5/2}\ FM_F=0\rangle$ states of $^{43}Ca^+$ with $A=-1$.

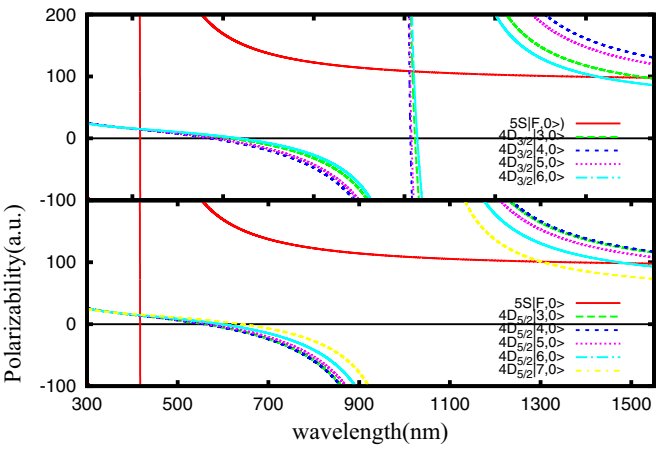

FIG. 5. F-dependent dynamic dipole polarizabilities (in a.u.) for the $|5S_{1/2}F,M_F=0\rangle$ ($F=4$,5) and $|4D_{3/2,5/2}\ F,M_F=0\rangle$ states of $^{87}Sr^+$ with $A=-1$.

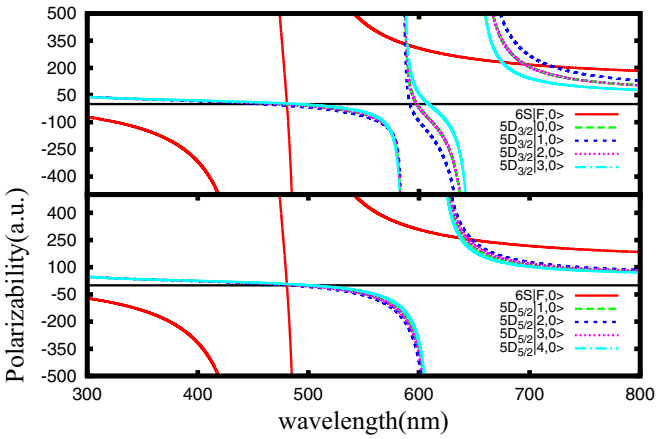

FIG. 6. F-dependent dynamic dipole polarizabilities (in a.u.) for the $|6S_{1/2}F,M_F0\rangle$ ($F=1,2$) and $|5D_{3/2,5/2}\ F,M_F=0\rangle$ states of $^{137}Ba^+$ with $A=-1$.

transitions are obtained by locating the crossing points between the two polarizability curves. In Tables III, IV, V, and VI, we list the λ_{magic} for the considered transitions along with their respective uncertainties in the parentheses. The corresponding polarizability values at λ_{magic} are listed as well. The resonant wavelengths λ_{res} are listed in the same table to demonstrate placement of a λ_{magic} in between two resonant transitions. In this work, we use left-handed circularly polarized light ($A=-1$) for all purposes, considering all possible positive and negative M_J sublevels for the ground $S_{1/2}$ and $D_{3/2,5/2}$ states. Note that λ_{magic} for the right-circularly polarized light of a transition for a given M_J are equal to the λ_{magic} for left-circularly polarized light with opposite sign of M_J [46].

We also investigate λ_{magic} between the transitions involving the $|nS_{1/2}F,M_F=0\rangle$ and $|(n-1)D_{3/2,5/2}F,M_F=0\rangle$ states. The ac Stark shifts of the hyperfine levels of an atomic state are calculated using the method described in Sec. II. We choose $M_F=0$ sublevels in the hyperfine transitions for this particular magnetic sublevel, and the first-order Zeeman shift vanishes. This is advantageous for the optical clock experiments [4]. We show the λ_{magic} values of the $|nS_{1/2}F,M_F=0\rangle \rightarrow |(n-1)D_{3/2,5/2}F,M_F=0\rangle$ transitions in Figs. 4, 5, and 6 for the $^{43}Ca^+$, $^{87}Sr^+$, and $^{137}Ba^+$ ions respectively. These values are listed in Table VII and we discuss below about these results for the individual ion.

1. $^{43}Ca^+$

As evident from Fig. 1, the dynamic polarizabilities for the $4S_{1/2}$ state are small except in the vicinity of the resonant $4S_{1/2}$-$4P_{1/2}$ and $4S_{1/2}$-$4P_{3/2}$ transitions around 396.847 and 393.366 nm respectively. Since the $3D_{3/2,5/2}$ states have significant contributions from the resonances in the interested wavelength range, the λ_{magic} are expected to lie in between these resonances. We found a total of nine λ_{magic} for all possible magnetic sublevels of the $4S_{1/2}$-$3D_{3/2}$ transition in between four resonances. The first four λ_{magic} are located around 395 nm between the resonant $4S_{1/2}$-$4P_{1/2}$ and $4S_{1/2}$-$4P_{3/2}$ transitions for all the M_J magnetic sublevels of the $4D_{3/2}$ state. Out of these, two λ_{magic} support blue-detuned trap, whereas the other two support red-detuned trap. The next five λ_{magic} are identified at 850.9(2), 853.1(2), 1467.8(4), 1013.4(5), and 870.7(3) nm, which lie in the infrared region. For some of the M_J sublevels, the λ_{magic} is missing. In such cases, it would be imperative to consider a geometry where λ_{magic} will be independent of the magnetic sublevels as mentioned in Sec. I and discussed elaborately in our previous work [47,48]. In Table V, we present the λ_{magic} for the $4S_{1/2}$-$3D_{5/2}$ transition considering all the magnetic sublevels of the $3D_{5/2}$ state. As seen, most of these λ_{magic} in the $^{43}Ca^+$ ion support red-detuned trap, indicated by small positive values of the polarizabilities for the corresponding λ_{magic} values. Similarly, we tabulate λ_{magic} for the $4S$ ($M_J=-1/2$)–$3D_{3/2,5/2}$ transition in Tables IV and VI. It can be evidently seen from the table that λ_{magic} are red shifted from the λ_{magic} for $4S$ ($M_J=1/2$)–$3D_{3/2,5/2}$.

Similarly in Table VII, we list the λ_{magic} values between 300 and 1300 nm for the $|4S_{1/2}F,M_F=0\rangle \rightarrow |3D_{3/2,5/2}F,M_F=0\rangle$ transitions. The F-dependent polarizabilities values at the respective λ_{magic} are listed as well. For this wavelength range, a total of 24 λ_{magic} are located, out of which 14 λ_{magic} are identified in the infrared region. From this table, it can be found that for the $|4S_{1/2}F,M_F=0\rangle \rightarrow |3D_{3/2,5/2}F,M_F=0\rangle$ transitions, all λ_{magic} support red-detuned traps.

2. $^{87}Sr^+$

The dynamic polarizabilities for the $5S_{1/2}$, $4D_{3/2}$, and $4D_{5/2}$ states of $^{87}Sr^+$ calculated by us are plotted in Fig. 2. A number of λ_{magic} are identified by the intersections of the polarizability curves of the $5S_{1/2}$ and $4D_{3/2,5/2}$ states for all their magnetic sublevels of the $4D_{3/2,5/2}$ states in the $5S_{1/2}(M_J=1/2)$–$4D_{3/2,5/2}$ transitions and are presented in Table III along with their resonant lines. Four λ_{magic} are found to be around 413 nm between the $5S_{1/2}$-$5P_{1/2}$ and $5S_{1/2}$-$5P_{3/2}$, resonant transitions. These values belong to the visible region, while the other five λ_{magic} are located at 1009.3(3), 1019.7(3), 1062.5(3), and 1577.2(3) nm that lie in the infrared region. All the λ_{magic} values mentioned for the $5S_{1/2}$-$4D_{3/2}$ transition, except for the one at 412.5(9) nm, support the red-detuned trapping scheme. Similarly, for the $5S_{1/2}$-$4D_{5/2}$ transition, a total of eight λ_{magic} are appearing for all possible M_J sublevels. Among them, two λ_{magic} are located at 1379.4(3) and 1130.8(4) nm and appear after the $4D_{5/2}$-$5P_{3/2}$ resonance for the $M_J=1/2$ and $M_J=-1/2$ magnetic sublevels respectively. Use of these λ_{magic} are recommended to carry out experiments selectively for the corresponding magnetic sublevels. Similarly, we present λ_{magic} for the $5S$ ($M_J=-1/2$)–$4D_{3/2,5/2}$ transition in Tables IV and VI. It can be noticed from these tables that λ_{magic} are red shifted from the λ_{magic} for $5S$ ($M_J=1/2$)–$4D_{3/2,5/2}$ transition. We have also determined total 16 extra λ_{magic} between $5S_{1/2}$-$5P_{1/2}$ and $4D_{3/2}$-$5P_{3/2}$ resonance transition.

In Table VII, λ_{magic} values above 300 nm are listed in the case of $^{87}Sr^+$ for the $|5S_{1/2}F,M_F=0\rangle \rightarrow |4D_{3/2,5/2}F,M_F=0\rangle$ transitions. It is found that λ_{magic} around 417 nm with very small polarizabilities for the $|5S_{1/2}FM_F=0\rangle \rightarrow |4D_{3/2}F,M_F=0\rangle$ and $|5S_{1/2}FM_F=0\rangle \rightarrow |4D_{5/2}F,M_F=0\rangle$ transitions. Therefore, it will be challenging to trap the $^{87}Sr^+$ ion at these wavelengths. However, the λ_{magic} values in the infrared region for these transitions may be useful for trapping the above ion in the experiments.

TABLE VII. The λ_{magic} values (in nm) and their corresponding polarizabilities $\alpha_d^F(\lambda_{\text{magic}})$ (in a.u.) for the $nS_{1/2}|\ F,M_F\rangle \rightarrow (n-1)D_{3/2,5/2}|\ F',M_{F'}\rangle$ transitions in $^{43}Ca^+$ ($I = 7/2$), $^{87}Sr^+$ ($I = 9/2$), and $^{137}Ba^+$ ($I = 3/2$).

	$^{43}Ca^+$				
	$4S_{1/2}$-$3D_{3/2}$			$4S_{1/2}$-$3D_{5/2}$	
$\lvert F,M_F\rangle \rightarrow \lvert F',M_{F'}\rangle$	λ_{magic}	$\alpha_d^F(\lambda_{\text{magic}})$	$\lvert F,M_F\rangle \rightarrow \lvert F',M_{F'}\rangle$	λ_{magic}	$\alpha_d^F(\lambda_{\text{magic}})$
$\lvert 3,0\rangle \rightarrow \lvert 2,0\rangle$	395.79(2)	8.69	$\lvert 3,0\rangle \rightarrow \lvert 1,0\rangle$	395.79(3)	3.35
	852.5(2)	95.86		992(4)	89.71
	999(4)	89.46	$\lvert 3,0\rangle \rightarrow \lvert 2,0\rangle$	395.79(3)	3.35
$\lvert 3,0\rangle \rightarrow \lvert 3,0\rangle$	395.79(2)	3.35		1077(9)	87.31
	851.3(2)	95.95	$\lvert 3,0\rangle \rightarrow \lvert 3,0\rangle$	395.79(3)	3.35
	1089(7)	87.02		1064(9)	87.61
$\lvert 3,0\rangle \rightarrow \lvert 4,0\rangle$	395.79(4)	3.35	$\lvert 3,0\rangle \rightarrow \lvert 4,0\rangle$	395.78(3)	3.35
	851.7(2)	95.92		1032(7)	88.48
	1049(4)	87.99	$\lvert 3,0\rangle \rightarrow \lvert 5,0\rangle$	395.79(3)	3.35
$\lvert 3,0\rangle \rightarrow \lvert 5,0\rangle$	395.79(2)	8.69		992(4)	89.71
	853.4(2)	95.82	$\lvert 4,0\rangle \rightarrow \lvert 6,0\rangle$	395.79(3)	8.69
	970(3)	90.44		949(3)	91.21
	$^{87}Sr^+$				
	$5S_{1/2}$-$4D_{3/2}$			$5S_{1/2}$-$4D_{5/2}$	
$\lvert F,M_F\rangle \rightarrow \lvert F',M_{F'}\rangle$	λ_{magic}	$\alpha_d^F(\lambda_{\text{magic}})$	$\lvert F,M_F\rangle \rightarrow \lvert F',M_{F'}\rangle$	λ_{magic}	$\alpha_d^F(\lambda_{\text{magic}})$
$\lvert 4,0\rangle \rightarrow \lvert 3,0\rangle$	416.99(8)	14.79	$\lvert 4,0\rangle \rightarrow \lvert 3,0\rangle$	416.99(8)	13.72
	1017.4(3)	108.24	$\lvert 4,0\rangle \rightarrow \lvert 4,0\rangle$	416.99(7)	13.72
	1534(30)	97.96	$\lvert 4,0\rangle \rightarrow \lvert 5,0\rangle$	416.99(8)	14.14
$\lvert 4,0\rangle \rightarrow \lvert 4,0\rangle$	416.99(8)	13.87	$\lvert 4,0\rangle \rightarrow \lvert 6,0\rangle$	416.99(8)	14.56
	1010.7(5)	108.52		1486(32)	98.45
$\lvert 4,0\rangle \rightarrow \lvert 5,0\rangle$	416.99(7)	14.15	$\lvert 5,0\rangle \rightarrow \lvert 7,0\rangle$	416(3)	14.56
	1012.4(6)	108.45		1301(14)	100.88
$\lvert 4,0\rangle \rightarrow \lvert 6,0\rangle$	416.99(7)	14.99			
	1020.6(2)	108.12			
	1429(20)	99.08			
	$^{137}Ba^+$				
	$6S_{1/2}$-$5D_{3/2}$			$6S_{1/2}$-$5D_{5/2}$	
$\lvert F,M_F\rangle \rightarrow \lvert F',M_{F'}\rangle$	λ_{magic}	$\alpha_d^F(\lambda_{\text{magic}})$	$\lvert F,M_F\rangle \rightarrow \lvert F',M_{F'}\rangle$	λ_{magic}	$\alpha_d^F(\lambda_{\text{magic}})$
$\lvert 1,0\rangle \rightarrow \lvert 0,0\rangle$	480.6(7)	−2.79	$\lvert 1,0\rangle \rightarrow \lvert 1,0\rangle$	480.53(3)	5.36
	588.3(2)	329.33		641.2(5)	256.97
	695.7(9)	219.39			
$\lvert 1,0\rangle \rightarrow \lvert 1,0\rangle$	480.7(4)	−9.37	$\lvert 1,0\rangle \rightarrow \lvert 2,0\rangle$	480.58(4)	0.91
	587.3(3)	331.55		647.8(6)	251.11
	720.47(2)	207.98			
$\lvert 1,0\rangle \rightarrow \lvert 2,0\rangle$	480.68(4)	−2.88	$\lvert 1,0\rangle \rightarrow \lvert 3,0\rangle$	480.55(4)	3.39
	588.3(5)	329.33		644.1(5)	254.42
	695.7(5)	219.40			
$\lvert 1,0\rangle \rightarrow \lvert 3,0\rangle$	480.56(4)	3.55	$\lvert 2,0\rangle \rightarrow \lvert 4,0\rangle$	480.56(5)	7.84
	589.7(4)	329.62		637.7(3)	260.25
	675.4(5)	231.02			

3. $^{137}Ba^+$

A total of nine λ_{magic} are found for the $6S_{1/2}$-$5D_{3/2}$ transition of $^{137}Ba^+$, among which four λ_{magic} are around 468 nm in the vicinity of the $6S_{1/2}$-$6P_{3/2}$ resonant transition. The next λ_{magic} at 587.6(9), 589.5(3), and 589.6(5) nm are located at the sharp intersection of polarizability curves close to the $5D_{3/2}$-$6P_{3/2}$ and $5D_{3/2}$-$6P_{1/2}$ resonances, as seen in Fig. 6. The last two λ_{magic} are located at 841.7(5) and 690.7(7) nm for the $M_J = 3/2$ and $1/2$ sublevels, respectively, and have positive polarizabilities. Hence, these λ_{magic} could provide sufficient trap depth at the reasonable laser power. In fact, some of the expected λ_{magic} are missing for the $M_J = -3/2$ and $-1/2$ sublevels. Similarly, several λ_{magic} are also located for the $6S_{1/2}$-$5D_{5/2}$ transitions, as seen from Fig. 6, in the wavelength range 300–800 nm, which are listed in Table V. The expected trend of locating λ_{magic} between the resonances in this transition is similar to the previous two ions. For the $6S$ ($M_J = -1/2$)–$5D_{3/2,5/2}$ transition, we list the λ_{magic} in Tables IV and VI. These magic wavelengths are slightly red shifted to those demonstrated for $6S$ ($M_J = -1/2$)–$5D_{3/2,5/2}$ transition. We also found a total of 15 λ_{magic} between $6S_{1/2}$-$6P_{1/2}$ and $5D_{3/2}$-$6P_{1/2}$ resonance transitions in both the

TABLE VIII. The λ_T values (in nm) for all possible magnetic sublevels M_J of the $^{43}Ca^+$,$^{87}Sr^+$, and $^{137}Ba^+$ alkaline-earth-metal ions using circularly polarized light.

$^{43}Ca^+$			$^{87}Sr^+$			$^{137}Ba^+$		
State	M_J	λ_T	State	M_J	λ_T	State	M_J	λ_T
$4S_{1/2}$	1/2	482.9	$5S_{1/2}$	–1/2	479.2	$6S_{1/2}$	–1/2	584.7
				–1/2	416.8		–1/2	478.3
				–1/2	442.3		–1/2	504.9
				1/2	417.2		1/2	482.9
$3D_{3/2}$	–1/2	746.2	$4D_{3/2}$	–1/2	881.5	$5D_{3/2}$	–1/2	551.6
	1/2	853.9		1/2	1024.7		1/2	424.4
	3/2	851.2		1/2	467.6		3/2	590.0
				3/2	1010.1			
$3D_{5/2}$	–1/2	690.2	$4D_{5/2}$	–1/2	834.5	$5D_{5/2}$	–1/2	571.5
	1/2	434.5		1/2	525.6		1/2	489.3
							3/2	417.5

tables. We have also determined an extra λ_{magic} at 590.5 nm in Table IV, which supports a red-detuned trap.

In Table VII, we also list λ_{magic} for the $|6S_{1/2}F,M_F = 0\rangle \rightarrow |5D_{3/2,5/2}F,M_F = 0\rangle$ transitions which lie within the wavelength range of 300–800 nm. We correspondingly locate 20 λ_{magic} in the visible region. We notice that all the λ_{magic} values, except around 480 nm, are expected to be more promising for experiments. An ion trap at these wavelengths can have sufficient trap depth at the reasonable laser power.

4. Tune-out wavelengths

Tables VIII and IX illustrate the identified tune-out wavelengths of the $nS_{1/2}$, $(n-1)D_{3/2}$, and $(n-1)D_{5/2}$ states in the (J,M_J) and (F,M_F) levels of the $^{43}Ca^+$, $^{87}Sr^+$, and $^{137}Ba^+$ alkaline-earth-metal ions. To locate these tune-out wavelengths, we have calculated the dynamic polarizabilities

TABLE IX. The λ_T values (in nm) for F hyperfine levels ($M_F = 0$) of the $^{43}Ca^+$,$^{87}Sr^+$, and $^{137}Ba^+$ alkaline-earth-metal ions using circularly polarized light.

$^{43}Ca^+$			$^{87}Sr^+$			$^{137}Ba^+$		
State	F	λ_T	State	F	λ_T	State	F	λ_T
$4S_{1/2}$	3	482.9	$5S_{1/2}$	4	417.1	$6S_{1/2}$	1	480.5
$3D_{3/2}$	2	505.7	$4D_{3/2}$	3	616.3	$5D_{3/2}$	0	472.3
		853.4			1023.2			597.9
	3	467.3		4	570.7		1	456.6
		881.6			1012.9			591.9
	4	480.8		5	583.2		2	472.4
		852.2			1015.5			597.9
	5	526.4		6	634.8		3	491.3
		854.5			1028.5			608.7
$3D_{5/2}$	1	495.8	$4D_{5/2}$	3	560.4	$5D_{5/2}$	1	552.5
	2	456.1		4	557.9		2	509.5
	3	460.2		5	570.9		3	519.2
	4	473.5		6	596.8		4	527.1
	5	495.8		7	641.9			
	6	532.5						

TABLE X. The λ_{magic} values (in nm) independent of M_J, F, and M_F with their corresponding polarizabilities (in a.u.) for the $nS_{1/2}$–$(n-1)D_{3/2,5/2}$ transition in the $^{43}Ca^+$,$^{87}Sr^+$, and $^{137}Ba^+$ ions with $n = 4,5,6$ respectively.

Ca^+ $4S_{1/2}$-$3D_{3/2}$		Sr^+ $5S_{1/2}$-$4D_{3/2}$		Ba^+ $6S_{1/2}$-$5D_{3/2}$	
λ_{magic}	$\alpha^J_{d,0}(\lambda_{magic})$	λ_{magic}	$\alpha^J_{d,0}(\lambda_{magic})$	λ_{magic}	$\alpha^J_{d,0}(\lambda_{magic})$
395.82(3)	4.90	416.9(3)	14.47	480.6(5)	–2.89
852.45(2)	95.87	1014.6(2)	108.35	588.4(3)	329.33
1029.7(2)	88.55			655.50(3)	244.89
$4S_{1/2}$-$3D_{5/2}$		$5S_{1/2}$-$4D_{5/2}$		$6S_{1/2}$-$5D_{5/2}$	
395.82(2)	4.20	416.9(3)	13.3	480.6(4)	–3.75
1014.10(3)	89.01	1566.2(3)	97.63	695.7(3)	219.4

of the above states for a particular range of wavelength in the vicinity of relevant resonances for the corresponding ion and find out values of λ for which the polarizability values tend to zero.

D. Magnetic sublevel independent λ_{magic} and λ_T

We have also used our the frequency-dependent scalar polarizability results of the $^{43}Ca^+$, $^{87}Sr^+$, and $^{137}Ba^+$ ions to find out λ_{magic} that are independent of the magnetic sublevels M_J of the atomic states and so are also hyperfine sublevel independent. Table X lists the λ_{magic} values for the $nS_{1/2}$-$(n-1)D_{3/2,5/2}$ transitions, which lie within the wavelength range of 300–1500 nm. We are also able to locate the tune-out wavelengths of the ground, $(n-1)D_{3/2}$, and $(n-1)D_{5/2}$ states of the considered alkaline ions that are independent of the F, M_F, and M_J values of the respective ion and given them in Table XI. Occurrences of these λ_{magic} and λ_T for the considered ions can offer pathways to carry out many high-precision measurements with minimal systematics.

V. CONCLUSION

We have determined scalar, vector, and tensor polarizabilities of the $nS_{1/2}$, $(n-1)D_{3/2}$, and $(n-1)D_{5/2}$ states in the $^{43}Ca^+$, Sr^+, and $^{137}Ba^+$ alkaline-earth-metal ions with the ground-state principal quantum number n. We used very precise values of the electric dipole matrix elements that are obtained them by employing a relativistic all-order method.

TABLE XI. The λ_T values (in nm) independent of M_J, F, and M_F for the $nS_{1/2}$, $(n-1)D_{3/2}$, and $(n-1)D_{5/2}$ states of the $^{43}Ca^+$,$^{87}Sr^+$, and $^{137}Ba^+$ ions with $n = 4,5,6$ respectively.

$^{43}Ca^+$		$^{87}Sr^+$		$^{137}Ba^+$	
State	λ_T	State	λ_T	State	λ_T
$4S_{1/2}$	395.796	$5S_{1/2}$	417.025	$6S_{1/2}$	480.596
$3D_{3/2}$	492.572	$4D_{3/2}$	598.633	$5D_{3/2}$	472.461
	852.776		1018.873		597.983
$3D_{5/2}$	482.642	$4D_{5/2}$	585.677	$5D_{5/2}$	509.687

Nondominant contributions in the adopted sum-over-states approach for the evaluation of the polarizabilities are estimated using lower order perturbation methods. The obtained static polarizability values are compared with the other available theoretical results and experimental values to gauge their accuracies. Dynamic polarizabilities at 1064 nm are given explicitly for the $nS_{1/2}$ and $(n-1)D_{3/2,5/2}$ states of the considered alkaline-earth-metal ions, which could help in creating high-field-seeking traps using the Nd:YAG laser. Furthermore, using the dynamic polarizabilities for a wide range of wavelengths, we have located a number of tune-out wavelengths λ_T of the above states and the magic wavelengths λ_{magic} for the $|nS_{1/2}F, M_F = 0\rangle \rightarrow |(n-1)D_{3/2,5/2}F, M_F = 0\rangle$ clock transitions due to the circularly polarized light in the $^{43}Ca^+$, $^{87}Sr^+$, and $^{137}Ba^+$ alkaline-earth-metal ions. We have located a significant number of λ_{magic} for these clock transitions, which can help the experimentalists to trap the above ions and reduce uncertainties in the clock transitions due to Stark shifts. This knowledge would also be of immense interest to carry out other high-precision studies using the considered ions. In addition, we have also determined the λ_{magic} and λ_T values that are independent of the choice of magnetic and hyperfine sublevels of the above clock transitions.

ACKNOWLEDGMENTS

The work of B.A. is supported by Department of Science and Technology, India, and the work of J.K. is supported by UGC-BSR Grant No. F.7-273/2009/BSR, India. S.S. acknowledges financial support from UGC-BSR. A part of the computations was carried out using Vikram-100 HPC cluster of Physical Research Laboratory and the employed SD method was developed in the group of Professor M. S. Safronova of the University of Delaware, USA.

[1] N. Poli, M. Schioppo, S. Vogt, S. Falke, U. Sterr, C. Lisdat, and G. M. Tino, Appl. Phys. B **117**, 1107 (2014).
[2] T. Nicholson, S. Campbell, R. Hutson, G. Marti, B. Bloom, R. McNally, W. Zhang, M. Barrett, M. Safronova, G. Strouse *et al.*, Nat. Commun. **6**, 6896 (2015).
[3] H. Katori, T. Ido, and M. K. Gonokami, J. Phys. Soc. Jpn. **68**, 2479 (1999).
[4] C. Champenois, M. Houssin, C. Lisowski, M. Knoop, G. Hagel, M. Vedel, and F. Vedel, Phys. Lett. A **331**, 298 (2004).
[5] C. W. Chou, D. B. Hume, J. C. J. Koelemeij, D. J. Wineland, and T. Rosenband, Phys. Rev. Lett. **104**, 070802 (2010).
[6] H. S. Margolis, G. P. Barwood, G. Huang, H. A. Klein, S. N. Lea, K. Szymaniec, and P. Gill, Science **306**, 1355 (2004).
[7] E. Peik, B. Lipphardt, H. Schnatz, T. Schneider, C. Tamm, and S. G. Karshenboim, Laser Phys. **15**, 1028 (2005).
[8] T. Rosenband, D. B. Hume, P. O. Schmidt, C. W. Chou, A. Brusch, L. Lorini, W. H. Oskay, R. E. Drullinger, T. M. Fortier, J. E. Stalnaker, S. A. Diddams, W. C. Swann, N. R. Newbury, W. M. Itano, D. J. Wineland, and J. C. Bergquist, Science **319**, 1808 (2008).
[9] J. E. Stalnaker, S. A. Diddams, T. M. Fortier, K. Kim, L. Hollberg, J. C. Bergquist, W. M. Itano, M. J. Delany, L. Lorini, W. H. Oskay, T. P. Heavner, S. R. Jefferts, F. Levi, T. E. Parker, and J. Shirley, Appl. Phys. B **89**, 167 (2007).
[10] P. L. Liu, Y. Huang, W. Bian, H. Shao, H. Guan, Y. B. Tang, C. B. Li, J. Mitroy, and K. L. Gao, Phys. Rev. Lett. **114**, 223001 (2015).
[11] S. G. Karshenboim and E. Peik, *Astrophysics, Clocks, and Fundamental Constants* (Springer, Berlin, 2004).
[12] C. A. Sackett, D. Kielpinski, B. E. King, C. Langer, V. Meyer, C. J. Myatt, M. Rowe, Q. A. Turchette, W. M. Itano, D. J. Wineland *et al.*, Nature (London) **404**, 256 (2000).
[13] T. Hong, C. Cramer, E. Cook, W. Nagourney, and E. N. Fortson, Opt. Lett. **30**, 2644 (2005).
[14] J. Kaur, S. Singh, B. Arora, and B. K. Sahoo, Phys. Rev. A **92**, 031402(R) (2015).
[15] B. K. Sahoo, R. G. E. Timmermans, B. P. Das, and D. Mukherjee, Phys. Rev. A **80**, 062506 (2009).
[16] J. Sherman, W. Trimble, S. Metz, W. Nagourney, and N. Fortson, *2005 Digest of the LEOS Summer Topical Meetings* (IEEE, New York, 2005), p. 99.
[17] B. K. Sahoo, B. P. Das, R. K. Chaudhuri, D. Mukherjee, R. G. E. Timmermans, and K. Jungmann, Phys. Rev. A **76**, 040504(R) (2007).
[18] S. Burd, D. Leibfried, A. C. Wilson, and D. J. Wineland, Proc. SPIE **9349**, 93490 (2015).
[19] S. Singh, B. K. Sahoo, and B. Arora, Phys. Rev. A **93**, 063422 (2016).
[20] M. Hobein, A. Solders, M. Suhonen, Y. Liu, and R. Schuch, Phys. Rev. Lett. **106**, 013002 (2011).
[21] K. D. Bonin and V. V. Kresin, *Electric-Dipole Polarizabilities of Atoms, Molecules and Clusters* (World Scientific, Singapore, 1997).
[22] N. Manakov, V. Ovsiannikov, and L. Rapoport, Phys. Rep. **141**, 319 (1986).
[23] K. Beloy, Ph.D. thesis, University of Nevada, Reno, USA, 2009.
[24] V. V. Flambaum, V. A. Dzuba, and A. Derevianko, Phys. Rev. Lett. **101**, 220801 (2008).
[25] B. Arora, M. S. Safronova, and C. W. Clark, Phys. Rev. A **84**, 043401 (2011).
[26] L. J. LeBlanc and J. H. Thywissen, Phys. Rev. A **75**, 053612 (2007).
[27] B. Arora, D. K. Nandy, and B. K. Sahoo, Phys. Rev. A **85**, 012506 (2012).
[28] J. Kaur, D. K. Nandy, B. Arora, and B. K. Sahoo, Phys. Rev. A **91**, 012705 (2015).
[29] A. Kramida, Y. Ralchenko, J. Reader, and N. A. Team, NIST Atomic Spectra Database, ver. 5.2 (2014) http://physics.nist.gov/asd.
[30] Y. Singh, B. K. Sahoo, and B. P. Das, Phys. Rev. A **88**, 062504 (2013).
[31] B. K. Sahoo, L. W. Wansbeek, K. Jungmann, and R. G. E. Timmermans, Phys. Rev. A **79**, 052512 (2009).
[32] S. A. Blundell, W. R. Johnson, and J. Sapirstein, Phys. Rev. A **43**, 3407 (1991).
[33] W. R. Johnson, M. Idrees, and J. Sapirstein, Phys. Rev. A **35**, 8 (1987).

[34] M. S. Safronova, A. Derevianko, and W. R. Johnson, Phys. Rev. A **58**, 1016 (1998).
[35] M. S. Safronova and W. R. Johnson, Adv. At. Mol. Opt. Phys. **55**, 191 (2007).
[36] See Supplemental Material at http://link.aps.org/supplemental/10.1103/PhysRevA.95.042501 for more information about the electric matrix elements between many low-lying excited states of the considered alkaline-earth ions that are used in the evaluation of the dipole polarizabilities.
[37] Y. B. Tang, H. X. Qiao, T. Y. Shi, and J. Mitroy, Phys. Rev. A **87**, 042517 (2013).
[38] B. K. Sahoo, B. P. Das, and D. Mukherjee, Phys. Rev. A **79**, 052511 (2009).
[39] J. Mitroy and J. Y. Zhang, Eur. Phy. J. D. **46**, 415 (2008).
[40] E. S. Chang, J. Phys. B **16**, 539 (1983).
[41] J. Mitroy, J. Y. Zhang, and M. W. J. Bromley, Phys. Rev. A **77**, 032512 (2008).
[42] P. S. Barklem and B. J. O'Mara, Mon. Not. R. Astron. Soc. **311**, 535 (2000).
[43] E. L. Snow and S. R. Lundeen, Phys. Rev. A **76**, 052505 (2007).
[44] M. S. Safronova and U. I. Safronova, Phys. Rev. A **83**, 012503 (2011).
[45] Y. J. Chen, L. F. Goncalves, and G. Raithel, Phy. Rev. A **92**, 060501(R) (2015).
[46] S. Singh, K. Kaur, B. K. Sahoo, and B. Arora, J. Phys. B **49**, 145005 (2016).
[47] B. Arora and B. K. Sahoo, Phys. Rev. A **86**, 033416 (2012).
[48] B. K. Sahoo and B. Arora, Phys. Rev. A **87**, 023402 (2013).